AIP | Journal of Applied Physics

# Effect of irregularities in the work function and field emission properties of metals

Thiago A. de Assis, R. F. S. Andrade, C. M. C. de Castilho, J. C. Losada, Rosa M. Benito et al.

Citation: J. Appl. Phys. 108, 114512 (2010); doi: 10.1063/1.3518511
View online: http://dx.doi.org/10.1063/1.3518511
View Table of Contents: http://jap.aip.org/resource/1/JAPIAU/v108/i11
Published by the AIP Publishing LLC.

# Effect of irregularities in the work function and field emission properties of metals

Thiago A. de Assis,[1,a)] R. F. S. Andrade,[2,b)] C. M. C. de Castilho,[3,c)] J. C. Losada,[4,d)] Rosa M. Benito,[4,e)] and F. Borondo[5,f)]
[1]*Departamento de Química, Universidad Autónoma de Madrid, Cantoblanco, 28049 Madrid, Spain and Departamento de Física y Mecánica, Grupo de Sistemas Complejos, ETSI Agrónomos, Universidad Politécnica de Madrid, Ciudad Universitaria, 28040 Madrid, Spain*
[2]*Instituto de Física, Universidade Federal da Bahia, Campus Universitário da Federação, Rua Barão de Jeremoabo s/n, 40170-115 Salvador-BA, Brazil*
[3]*Grupo de Física de Superfícies e Materiais, Instituto de Física and Instituto Nacional de Ciência e Tecnologia em Energia e Ambiente (CIENAM)INCT-E&A, Universidade Federal da Bahia, Campus Universitário da Federação, Rua Barão de Jeremoabo s/n, 40170-115 Salvador-BA, Brazil*
[4]*Departamento de Física y Mecánica, Grupo de Sistemas Complejos, ETSI Agrónomos, Universidad Politécnica de Madrid, Ciudad Universitaria, 28040 Madrid, Spain*
[5]*Departamento de Química, Universidad Autónoma de Madrid, Cantoblanco, 28049 Madrid, Spain and Instituto Mixto de Ciencias Matemáticas CSIC–UAM–UC3M–UCM, Universidad Autónoma de Madrid, Cantoblanco, 28049 Madrid, Spain*

(Received 24 August 2010; accepted 22 October 2010; published online 10 December 2010)

The effect of geometrical irregularities in the work function and emitting properties of metallic surfaces at low potentials is studied. For this purpose, we propose a simplified model consisting of rectangular fractures and a classical formalism for the work function determination. The dependence of the work function with the fractures size is determined by using the electrostatic image potential method. The emission current density properties when an external electric field is applied are also analyzed. © *2010 American Institute of Physics*. [doi:10.1063/1.3518511]

## I. INTRODUCTION

Until recently, the development of cold electron field emitters had not attracted much technological interest. This was mainly due to the fact that the existing devices, such as field ion or field emission microscopes, required a high operational voltage. The development of modern vacuum microelectronics changed the situation, since it made possible the construction of emitters able to operate at low voltages.[1,2]

An important property that significantly affects the emitting performance of a thin metal film is the work function (WF). This concept is related to the variation in the total energy of the metal sample when an electron in the Fermi level is removed. The WF is strongly affected by the conditions of the metal surface,[3] including, among other factors, the presence of contaminants (in quantities lower than one monolayer), the occurrence of oxidation and other chemical reactions, uneven distribution of adsorbates, or the crystallographic orientation.

In an early work on the thermoionic electron emission of metals, Smoluchowski[4] evaluated the WF differences associated with different crystallographic faces in tungsten, thus obtaining a satisfactory agreement with the scarce experimental data existing at that time. This author identified two major contributions of a given face to the WF; the first one being associated to the electronic atomic density in the bulk, while the second resulted from the last double layer on the metal surface. In this way, some general formulae for the double layers were derived for the simple cubic and body-centered cubic lattice, which allowed to characterize the stability of the surface configuration. Together with the formation of a dipole layer due to charge separation, these ideas were also used in other early works[5] to evaluate the potential drop and also to relate the combined effect of dipole interactions, surface structure, and adsorbate atoms in the value of the WF.[6]

In addition, it is well known that the microgeometry of the surfaces in actual electron emitters is far from being smooth. Even in the best cases, when the use of crystalline materials produces a smoother surface, it is important to take in consideration that the surface consists of the combination of several facets, that lead to an irregular surface at micrometric scale. Such irregularities, when occurring in metal structures subject to an external electric field, lead to an enhancement of the field in the neighborhood of sharp corners, edges, and tips.[7] For example, at the upper corner of a step due to a sharp edge there is a noticeable increase of the tunnelling rate, in such a way that this region is experimentally identified as a nucleation center.

With the aim of computationally simulate the geometrical defects associated to real metallic surfaces we studied, in a previous paper,[8] how the roughness and fractal dimension of a surface affect its electron emitting properties. We conclude that, the roughness has a significant influence in the electronic current density, while the fractal dimension is re-

[a)]Electronic mail: t.albuquerque@uam.es.
[b)]Electronic mail: randrade@ufba.br.
[c)]Electronic mail: caio@ufba.br.
[d)]Electronic mail: juancarlos.losada@upm.es.
[e)]Electronic mail: rosamaria.benito@upm.es.
[f)]Electronic mail: f.borondo@uam.es.

 

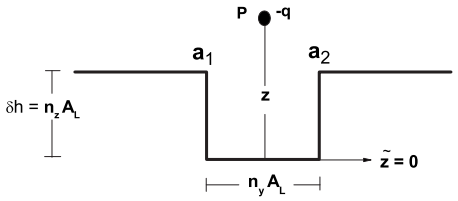


FIG. 1. Schematic of a fracture corresponding to the removal of atoms along a horizontal interval $n_yA_L$ with vertical dimension $n_zA_L$, being $n_y$ and $n_z$ integer numbers. The parameters of the model used for the determination of the image potential are shown. See text for details.

lated to the electric field enhancement factor. This information appeared embedded in the slope of the usual Fowler–Nordheim plots.

The aim of the present work is to analyze how the irregular geometry of a metallic surface affects the corresponding WF and determines its emitting properties. For this purpose, a simplified model formed by rectangular fractures together with a classical formalism for the determination of the WF is proposed.

As will be discussed in the next section, the classical method of image potential is particularly useful to determine how the WF at zero external electric field depends on the fracture size. For the evaluation of this magnitude, we consider the effect of the applied external electric field by solving Laplace's equation in the region limited by a cathode with irregular geometry and a distant planar anode. Once this solution is known the interaction energy between the electron and the surface at a distance $z_0$ from it can be easily computed. In addition, this method also permit the evaluation of the enhancement/reduction factors of the field due to the right angle corners at that upper and lower limits of the fracture. All these specific features are quite important for the evaluation of the electronic current density of a material with irregular geometry. The properties of the emission current density (ECD) when the metal is under the influence of an applied external electric field is subsequently computed with the help of an adapted formalism of field emission models, based on the methods proposed by Fowler–Nordheim,[9] Good–Muller,[10] and Forbes.[11,12] This model provides the framework to obtain a reasonable approximation for the elliptical functions, which are key elements of the Fowler–Nordheim theory.

The paper is organized as follows. In Sec. II the fracture model and the classical formalism for the WF determination are presented. Sec. III is devoted to the description and discussion of the obtained results, emphasizing the term associated to the fracture formation probability and its effect on the ECD. This permits to establish a relationship between the fracture distribution and the ECD evaluated along the profile. Finally, Sec. IV contains a summary of the most important results together with our concluding remarks.

## II. THEORY AND METHODS

### A. The fracture model and work function calculations

We consider that natural irregularities on crystalline faces, arise as a result of stable configurations of a fractured surface at room temperature (300 K), see Fig. 1.[13]

We will further assume that the lateral profile of the surface of an emitter presents a set of rectangular fractures, representing the fluctuations in the height of the profile. The isolated single straight steps on a cubic lattice are taken to be proportional to the value of the lattice parameter, $A_L$. In Fig. 1 we represent a profile of one such fracture corresponding to a "missing" profile portion of width $n_yA_L$ and depth $n_zA_L$, measured respectively along the horizontal and vertical directions, and being $n_y$ and $n_z$ integer numbers. We also consider the existence of an equipotential surface along the fracture border, something that can be justified by considering that the Debye radius for an electronic gas in metals is, in general, smaller than the metal lattice parameter.

We consider here a classical-Brodie-definition for the WF,[14] as the work necessary to move an electron against the forces of an image charge $\tau_{\text{image}}$. This definition leads to an expression for the WF that depends on the atomic radius, Fermi energy, and the effective electron mass. Halas *et al.*,[15] used this classic approach to compute metal surface WFs that were in excellent agreement with the experimental results, this corroborating that the above mentioned interpretation of the WF.

For the particular case of a flat surface held at a constant potential, the work required to move an electron from a point at a distance $z$ from the surface to infinity is given by

$$\tau_{\text{image}} = \int_z^{+\infty} \frac{e^2}{4\pi\epsilon_0(2z)^2} dz = \frac{e^2}{16\pi\epsilon_0 z}, \tag{1}$$

where $e$ is the elementary charge and $\epsilon_0$ is the vacuum permissivity in SI units. Equation (1) can be used to evaluate the reduced WF magnitude in a similar situation, where an uniform external electric field is applied between a flat metal surface and an anode placed very far from it. Indeed, the important issue in this case is the evaluation of the lower integration limit, $z$, as will be discussed later in this section. It is possible to advance that, for distances from the surface larger than a certain value $z=z_0$, classical mechanics could be used to determine to a very good approximation the value of the WF.[15] Moreover, the distance $z=z_0$ can be identified as the Heisenberg uncertainty distance that is required to pass by continuous decoherence from quantum to classical states.

From the exact results valid for some highly symmetric geometries, the method of image potential can be used to determine the zero field WF, $\phi^{\text{ZF}}_{n_y,n_z}$. For geometries of lower symmetry, as the one considered here with the presence of fractures, it is usually not possible to derive an exact solution for the potential outside the boundaries in terms of a finite number of image charges. However, it is possible to obtain approximate solutions if we evaluate how the deformations of the plane surface of a conductor modify the image potential. Let us first consider the simpler situation where no external electric field is applied. The method we developed for the determination of $\phi^{\text{ZF}}_{n_y,n_z}$ is based on the assumption that this quantity corresponds to the work done against the retarding force of electron image charge acting on the electron along its way out of the surface.[14] If we consider a point charge, $-q$, placed at the point $(x,y,z=z_0)$ above a conducting infinite plane $\tilde{z}=0$ (see Fig. 1), the required work $\delta\tau$ to

move it by an infinitesimal height, $\delta h(\tilde{x}_S,\tilde{y}_S)$ in the direction perpendicular to plane, due to the charges in a surface element $dS$, defined by the coordinates $(\tilde{x}_S,\tilde{y}_S)$, is given by the following:

$$\delta\tau = -\frac{1}{2}\delta h(\tilde{x}_S,\tilde{y}_S)\sigma(\tilde{x}_S,\tilde{y}_S)dSF_q^z(\tilde{x}_S,\tilde{y}_S), \tag{2}$$

where $\sigma(\tilde{x}_S,\tilde{y}_S)$ and $F_q^z(\tilde{x}_S,\tilde{y}_S)$ are the surface charge density and the electric field at $(\tilde{x}_S,\tilde{y}_S)$, respectively.

By Integrating Eq. (2) over the whole surface, and taking into account that $\sigma(\tilde{x}_S,\tilde{y}_S)=F_{\text{charge}}^z(\tilde{x}_S,\tilde{y}_S)\epsilon_0$, we obtain the following expression for the variation in the potential energy of the system:

$$\delta U_{\text{plane}} = \int \delta\tau = -\frac{\epsilon_0}{2}\int [F_q^z(\tilde{x}_S,\tilde{y}_S)]^2\delta h(\tilde{x}_S,\tilde{y}_S)dS. \tag{3}$$

From this equation and taking into account that $F_q^z(\tilde{x}_S,\tilde{y}_S)=-\nabla_z V$, it is straightforward to obtain

$$\delta U_{\text{plane}} = -\frac{\epsilon_0}{2}\int_{-\infty}^{+\infty}d\tilde{y}\int_{-\infty}^{+\infty}d\tilde{x}|\nabla_z V|_{\tilde{z}=0}^2\delta h, \tag{4}$$

where $V$ accounts for the electric potential on the plane caused by the actual and image charges. In this way, we have the following expression for $\delta U_{\text{plane}}$:

$$\begin{aligned}\delta U_{\text{plane}} &= -2\epsilon_0\delta h z^2 \\ &\quad\times\int_{-\infty}^{+\infty}d\tilde{y}\int_{-\infty}^{+\infty}d\tilde{x}\frac{q^2}{[(\tilde{x}-x)^2+(\tilde{y}-y)^2+z^2]^3} \\ &= -\frac{q^2}{16\pi\epsilon_0 z^2}\delta h.\end{aligned} \tag{5}$$

For an adequate discussion of the consequences of Eq. (5), it is useful to consider the exact result for the potential energy of the actual system (actual charge+plane), when the plane, originally at $\tilde{z}=0$, is displaced upwards by a small amount, $\delta h>0$. According to Eq. (1), the exact potential energy $U(z)$ in this case is given by

$$U(z) = -\frac{q^2}{16\pi\epsilon_0(z-\delta h)} = -\frac{q^2}{16\pi\epsilon_0 z}\left(1+\frac{\delta h}{z}+\ldots\right). \tag{6}$$

As can be seen, the first order correction, after the dominant contribution given by Eq. (1), to the potential energy of Eq. (6) coincides with the Eq. (5). This actually explains the contribution $\delta U_{\text{plane}}$.

In what follows, we will restrict our work to this first approximation when evaluating, due to the impossibility of finding exact image charge solution, $\phi_{n_y,n_z}^{\text{ZF}}$, to our problem. As one can easily see from the expansion of Eq. (6), the next contribution to the higher order terms is proportional to $(\delta h/z)^2$. Although $\delta h/z<1$, higher order terms might still contribute to $\phi_{n_y,n_z}^{\text{ZF}}$. This does not seems to be the case since our results (see next section) show that the previous first order approximation gives results in rather consistent agreement with experimental values.

If we represent surface fractures by the profile sketched in Fig. 1, the first order approximation of the potential energy of the new system $\delta U_{\text{frac}}$ can be written as

$$\begin{aligned}\delta U_{\text{frac}} &= -2\epsilon_0\delta h z^2\left[\int_{-\infty}^{a_1}d\tilde{y}+\int_{a_2}^{+\infty}d\tilde{y}\right] \\ &\quad\times\int_{-\infty}^{+\infty}d\tilde{x}\frac{q^2}{[(\tilde{x}-x)^2+(\tilde{y}-y)^2+z^2]^3},\end{aligned} \tag{7}$$

where the actual charge $-q$, placed at the point $(x,y,z=z_0)$ with respect to the bottom of the fracture $(\tilde{z}=0)$, does not contribute to the variation in the potential energy. According to Brodie's proposal [see Eq. (1)], the zero field WF of a rectangular fracture $\phi_{n_y,n_z}^{\text{ZF}}$, can be expressed, in an approximate way, by the expression

$$\phi_{n_y,n_z}^{\text{ZF}} \approx \left|-\frac{e^2}{16\pi\epsilon_0 z_0}+\delta U_{\text{frac}}\right|, \tag{8}$$

where $|q|=e$.

To go beyond this zero-field value, it is important to estimate the potential energy of an electron at a distance $z=z_0$ from the conducting surface in the presence of external electric field. To this end, we have numerically solved Laplace's equation with the iterative procedure developed in Ref. 16 using Dirichlet boundary conditions for an irregular cathode irregular with the profile shown in Fig. 1, and a plane anode far away from the cathode. In our case, the Dirichlet conditions are given by $V_{\text{cat}}=0$ and $V_{\text{an}}=100$ V. At both sides of the integration domain periodic lateral conditions are imposed so that for a domain formed by $L\times L\times K$ points (in the directions $x,y,z$, respectively) with $L\gg K$, so that

$$V_{i,j,k} = V_{i+L,j,k} = V_{i,j+L,k} = V_{i+L,j+L,k}. \tag{9}$$

Once the convergence of $V_{i,j,k}$ within the iterative procedure is achieved, it is possible to interpolate the solution to obtain the potential value at any off-grid point or, reversely, to obtain approximate values for the coordinates associated to a given value of the potential. The quality of these interpolations depends, of course, of the number of points that are used to construct the grid. Thus, it is possible to evaluate a set of equipotential surfaces for any chosen value of $V$. Let us consider the simple situation, where the potential variation rate between two successive grid points along the $\hat{\mathbf{k}}$ direction is

$$G_V = V_{i,j,k+1} - V_{i,j,k}, \tag{10}$$

The potential at an off-grid point $(i,j,k+dz)$ is given by

$$V_{i,j,k+dz} = V_{i,j,k} + G_V dz. \tag{11}$$

This method turns it possible to evaluate the electric potential at the point $P$ where the electric charge $-q$ is located (see Fig. 1). Therefore, the presence of the external field reduces the WF of the material by an amount $\Delta\phi$ given by:

$$\Delta\phi = -eV_P, \tag{12}$$

where $V_P$ corresponds to the electric potential at $P$.

Finally, we can estimate the WF of the material, $\phi^{\mathrm{mat}}_{n_y,n_z}$, including the image potential effect of its irregular geometry and the external electric field.

### B. Work function, field enhancement factor, and ECD

To compute the WF, $\phi^{\mathrm{mat}}_{n_y,n_z}$, we start from the following expression:

$$\phi^{\mathrm{mat}}_{n_y,n_z} \approx \phi^{\mathrm{ZF}}_{n_y,n_z} + \Delta\phi, \tag{13}$$

where $\phi^{\mathrm{ZF}}_{n_y,n_z}$ is determined from Eq. (8) and $\Delta\phi$ is determined by the Eq. (12).

Let us now evaluate the value of $z_0$, which was first introduced as the lower integration limit in Eq. (8), representing the smallest distance from the surface at where the electron can "feel" the influence of the image charges. According to Halas *et al.*,[15] a good agreement between theoretical values, according Brodie's WF definition, and the corresponding experimental values for metals and semi-metals is achieved when $z_0$ is chosen as

$$z_0 = \frac{a_0}{\sqrt{3}}\left(\frac{E_F}{\mathrm{Ryd}}\right)^{1/2}\left(\frac{r_s}{a_0}\right)^{3/2}. \tag{14}$$

In the above expression, $a_0$ and $E_F$ represent the Bohr radius and the Fermi energy, respectively, while $r_s$ is a density parameter related to the electron density, and 1 Ryd $=13.6058$ eV. Therefore, the necessary energy for the removal of an electron from a position $z_0$ above the surface to a point well far away from it is given by Eq. (13). In what follows we will take $n_z=1$, so that, for the sake of simplicity, we will write from now on that $\phi^{\mathrm{ZF}}_{n_y,n_z}=\phi^{\mathrm{ZF}}_{n_y}$ and $\phi^{\mathrm{mat}}_{n_y,n_z}=\phi^{\mathrm{mat}}_{n_y}$.

Let us remark that the electronic current density depends exponentially from the local electric field $F$, which in turn is strongly dependent on the material's geometry. The local electric field intensity is frequently expressed as an enhancement factor, $\gamma$, with respect to a constant reference field $F_0$, through the expression

$$F = \gamma F_0, \tag{15}$$

where $F_0$ represents a uniform electric field intensity determined from the potential, $V_{\mathrm{an}}$, of an equivalent anode assumed flat, and taking the electric potential value at the cathode equals to zero, $V_{\mathrm{cat}}=0$. For the determination of the ECD, $J$, we consider the Murphy–Good equation,[11,12,17] given by

$$J = [A(\phi^{\mathrm{mat}}_{n_y})^{-1}e^{\eta}(F_{\phi^{\mathrm{mat}}_{n_y}})^{\eta/6}]F^{(2-\eta/6)}\exp\left[-\frac{B(\phi^{\mathrm{mat}}_{n_y})^{3/2}}{F}\right], \tag{16}$$

where $F$ is the electric field, $F_{\phi^{\mathrm{mat}}_{n_y}}=\frac{4\pi\epsilon_0}{e^3}(\phi^{\mathrm{mat}}_{n_y})^2$, $\eta[\equiv B(\phi^{\mathrm{mat}}_{n_y})^{3/2}/F_{\phi^{\mathrm{mat}}_{n_y}}]$ is a constant and $A$ and $B$ are universal constants given by $A=e^3/8\pi h$ and $B=(8\pi/3)(2m_e)^{1/2}/eh$, respectively.[18]

Aiming at giving a more realistic simulation of the emitter boundary, we consider next a simple approximation for the ECD evaluation, which takes into account the formation of fractures, whose description was given in the previous section. For this purpose, a dynamical approach for the fracture formation is considered, which is based on a standard canonical distribution of fracture sizes. This approach, as described by Lapujoulade,[19] assumes a linear fracture density, $\lambda$, for a profile corresponding to the crystallographic face (100)

$$\lambda = \frac{2}{A_L}\exp\left(-\frac{w}{k_BT}\right), \tag{17}$$

where $w$ corresponds to the kink formation energy, $T$ is the absolute temperature, and $k_B$ is the Boltzmann constant. The factor 2 comes from the fact that the formation processes of either protrusions or depressions are equiprobable. Actually, the formation of a kink on the step of a surface is much less costly in energy than the creation of a defect on the corresponding terrace, i.e., an adatom or advacancy. Thus it is expected that, for a large temperature range, kinks on steps are the only defects being created. The occurrence probability of a fracture of width $n_yA_L$, $P_{n_y}$, will then be given by

$$P_{n_y} = p_1 p_2^{n_y} p_3, \tag{18}$$

where $p_1=p_3=\lambda A_L$ are the individual probabilities of the creation of a descending (ascending) kink. On the other hand, $p_2=1-2\lambda A_L$ represents the probability that no kinks are formed, i.e., the atoms keep the vertical position expressed by $n_z=1$. Hence, from Eqs. (17) and (18) it is possible to write

$$P_{n_y} = 4\exp\left(-\frac{2w}{k_BT}\right)\left[1-4\exp\left(-\frac{w}{k_BT}\right)\right]^{n_y}. \tag{19}$$

Notice that in the present approach for the field induced electronic emission no temperature effects, other than those derived from the Boltzmann weights, are taken into account. In our calculation we take $T=300$ K and $w=0.4$ eV, values for which $4\exp(-w/k_BT)\approx 7.6\cdot 10^{-7}\ll 1$, and then it is possible to approximate $P_{n_y}$ as

$$P_{n_y} \approx 4\exp\left(-\frac{2w}{k_BT}\right)\left[1-4n_y\exp\left(-\frac{w}{k_BT}\right)\right]. \tag{20}$$

We finally conclude the evaluation of the ECD within the models developed by Fowler–Nordheim and Murphy–Good. Accordingly, for a fracture $n_yA_L$ wide, with $(K-1)A_L \gg n_zA_L$, the previous considerations result in the following final expression for the local ECD, $J(n_y)_{i,j}$:

$$J(n_y)_{i,j} = \frac{P_{n_y}}{A_L^2}[A(\phi^{\mathrm{mat}}_{n_y})^{-1}e^{\eta}(F_{\phi^{\mathrm{mat}}_{n_y}})^{\eta/6}](\gamma_{i,j}F_0)^{(2-\eta/6)} \times \exp\left[-\frac{B(\phi^{\mathrm{mat}}_{n_y})^{3/2}}{(\gamma_{i,j}F_0)}\right]. \tag{21}$$

The total current, $J(n_y)$, of a surface with an $n_y$ fracture is

$$J(n_y) = \sum_{i,j=1}^{L\times L} J(n_y)_{i,j}. \tag{22}$$

One last comment is in order here. It is clear that when many fractures are present, their mutual interaction must be taken into account. In the present work, however, we consider that the distances between them are large enough to justify ne-

glecting the electrostatic interaction, coming from the interaction of electric dipoles. With this assumption, our methodology to calculate the WF is not compromised.

## III. RESULTS AND DISCUSSION

Let us now analyze how the fracture width, $n_y$, affects the value of the zero field WF, $\phi_{n_y}^{ZF}$. For this purpose, we initially compute $\phi_{\text{smooth}}$, corresponding to the case where no kink are present. We consider a silver (Ag) plane surface where the corresponding lattice parameter at low temperature is $A_L \approx 0.409$ nm,[20] the Fermi energy $E_F \approx 7.48$ eV, and the relation $r_s/a_0 \approx 2.39$.[15] Using Eqs. (14) and (1) it is possible to determine that in our case $\phi_{\text{smooth}} \approx 4.33$ eV, a very reasonable value when compared to the experimental one.[21] Our results show that the computed value of $\phi_{n_y}^{ZF}$ is almost insensitive to changes in the fracture size $n_y$ (relative change $\sim 10^{-4}$ when $n_y \in [5-100]$). For this calculation we have considered that the vertical displacement of the fractures is equal to the lattice parameter of the material. The value of $\phi_{n_y}^{\text{ZF}}$ depends more significantly on $n_y$ in the a smaller interval,[5–13] after which it asymptotically stabilizes to the $\phi_{\text{smooth}}$ value. We noticed that the range of variation is much smaller than expected from experimental considerations. Moreover, the high values of $\phi_{n_y}^{\text{ZF}}$ found for low values of $n_y$ are explained in our model as the result of an increment in the distance between the lateral sides at the fractures and the real electron charge position defined along the symmetry axis of the fracture $(0,[L-1]A_L/2,z_0)$. Another point worth commenting here is that, as can be seen, only values of $n_y \geq 5$ have been considered here (and also throughout the paper). The reason is simple. For smaller values of $n_y$ it would be necessary to take into account the (low) probability of fracture formation arising from the effect of the electrostatic repulsions between close kinks,[16] something which is outside the scope of the present work.

To evaluate the effect of the external field $F$ on the local WF for an electron located on the fracture symmetry axis, we first calculate the interaction energy between the electron at $z=z_0$ and the fracture' surface with the help of Eq. (12). In Fig. 2, we show how $\Delta\phi$ changes with respect to the fracture width, for which the values $n_y=5,19,21,23,25,255$ were selected. In this calculation, we chose the value of the anode electric potential, $V_{\text{an}}$, by imposing the condition that the homogeneous electric field at large distances from the surface be $F_0 \approx 10^7$ V/cm. As it is clearly illustrated by the results, the value $\Delta\phi$ is minimal when the electron is placed on the fracture symmetry axis, since this implies a reduction on the value of the WF, $\phi_{n_y}^{\text{mat}}$. This result allows to identify a preferential emission site in the central region of the fracture. At the same time, the results also show that the emission capacity is enhanced for larger values of $n_y$, until a limit value for $\Delta\phi$ is reached. In the example that we have considered, this corresponds to $\Delta\phi \approx -0.205$ eV, taking place for the largest considered value of $n_y=255$.

Moreover, our results suggest that step formation in metal surfaces reduces the corresponding WF, $\phi_{n_y}^{\text{mat}}$, by some tenths of eV. In Fig. 3 we show how the ratio between $\phi_{n_y}^{\text{mat}}$, given by Eq. (13), and $\phi_{\text{smooth}}$ changes with respect to the

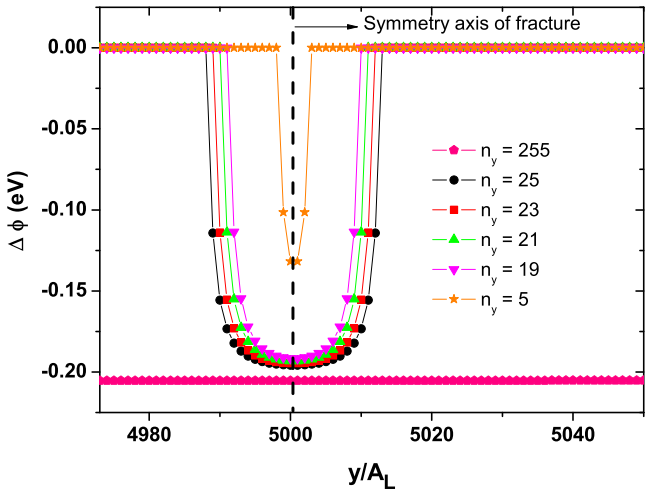


FIG. 2. (Color online) Variation in the metal work function in the neighborhood of the fractured surface for values of $n_y=5,19,21,23,25,255$. The vertical dashed line indicates the fracture symmetry axis. The points were obtained for an anode electric potential of $V_{\text{an}}=100$ V. For such value, the homogeneous electric field far away from the profile is $F_0 \approx 10^7$ V/cm.

fracture size. For example, for $n_y=255$, which corresponds in Ag to a fracture $n_y A_L=104.3$ nm wide, we obtain $\phi_{n_y=255}^{\text{mat}} \approx 4.126$ eV. Our results of Fig. 3 also indicate that the presence of fractures with smaller/larger width values have a significant effect by making the material emissive efficiency lower/higher, respectively. Before estimating this effect, it is necessary to evaluate the field distribution along the fracture surface.

To avoid large numeric fluctuations and possible overflows in the field calculation, we introduced an approximation corresponding to the replacement of the actual surface model with sharp square corners by an evaluated differentiable equipotential $V_{\text{eq}}$ staying as close as possible to the position to the surface. This is illustrated in Fig. 4, where the corresponding equipotential together with the sharp corner model for $V_{\text{eq}}=0.001V \approx V_{\text{cat}}$ is shown. Notice that both $x$ and $y$ change appreciably only on an extremely small length scale, so that for the evaluation of the field at the grid points, this equipotential represents an excellent approximation for the model surface.

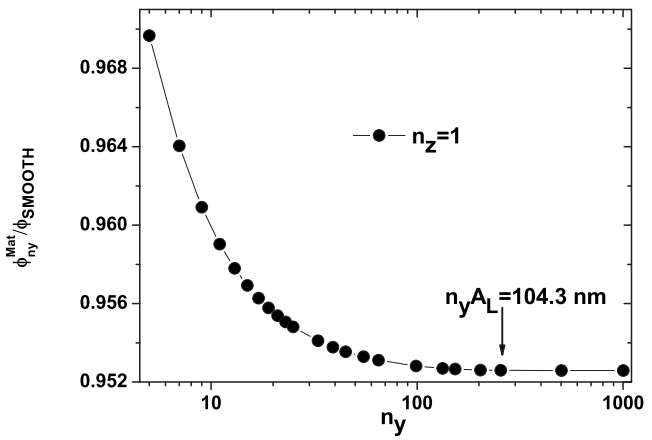


FIG. 3. Ratio $\phi_{n_y}^{\text{mat}}/\phi_{\text{smooth}}$ as a function of the fracture width, $n_y$. The arrow indicates the size $n_y A_L=104.3$ nm, which is already quite close to the asymptotic value $\phi_{n_y}^{\text{mat}}$. The anode electric potential $V_{\text{an}}$ value was the same as in Fig. 2.

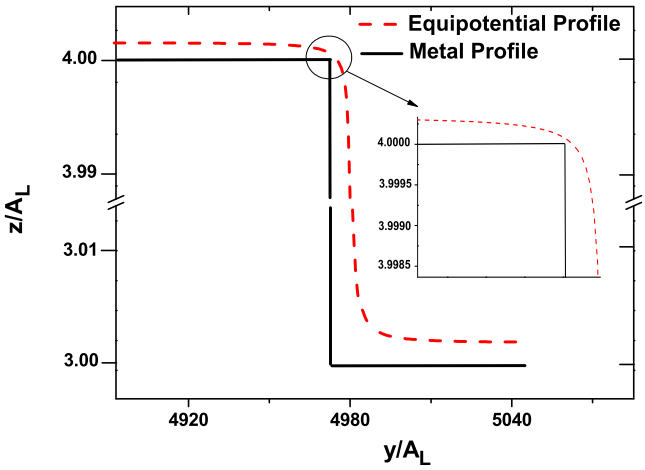


FIG. 4. (Color online) Equipotential line (dashed line) together with the sharp corner (solid line) model for $V_{eq}=0.001V \approx V_{cat}$.

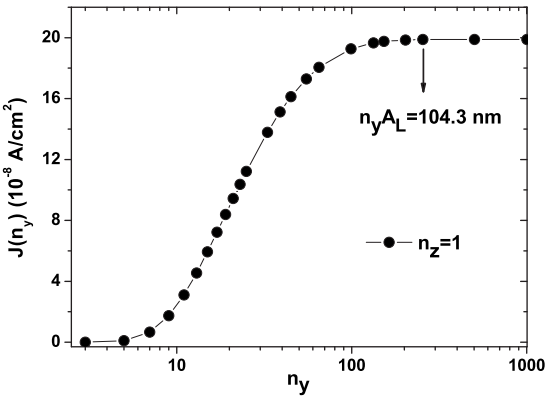


FIG. 6. Electronic current density as a function of the fracture width, $n_y$, (in logarithm scale) for a value of the external electric field of $F_0 \approx 10^7$ V/cm. The arrow indicates the optimal fracture width, i.e., the value leading to the largest value of the the total electronic current density.

We consider next how the enhancement factor, $\gamma$, defined in Eq. (15), changes in this particular region. The corresponding results are shown in Figs. 5(a) and 5(b), where the dependence for two values of the width, $n_y=5$ and 25, are plotted. As can be seen the smoothing approximation that has been introduced does not eliminate the large enhancement effect close to the corners, but conveniently avoid the expected logarithmic divergence of $\gamma$ at the corner.

When interpreting these results, it should be noticed that increasing the value of $n_y$ corresponds to an increase on the value of the local electric field, $F$, in the upper and lower corners and in the symmetry axis of the fracture. This can be interpreted as a result of the significant variation in the charge density taking place at the most protruding regions of the fracture. When the number of kinks per unit area gets higher it is reasonable to expect a more intense repulsion among charges of the same sign distributed along these regions, this leading to a reduction in the induced charge. The local enhancement factor approach site dependent asymptotic values, in such a way that, at the upper and lower fracture corners, as well as in the symmetry axis, they reach the specific values of $\gamma^{up} \approx 1.338$, $\gamma^{low} \approx 0.559$, and $\gamma^{sa} \approx 0.987$. As in the previous calculations, these values correspond to the largest fracture width $n_y=255$ considered in this work.

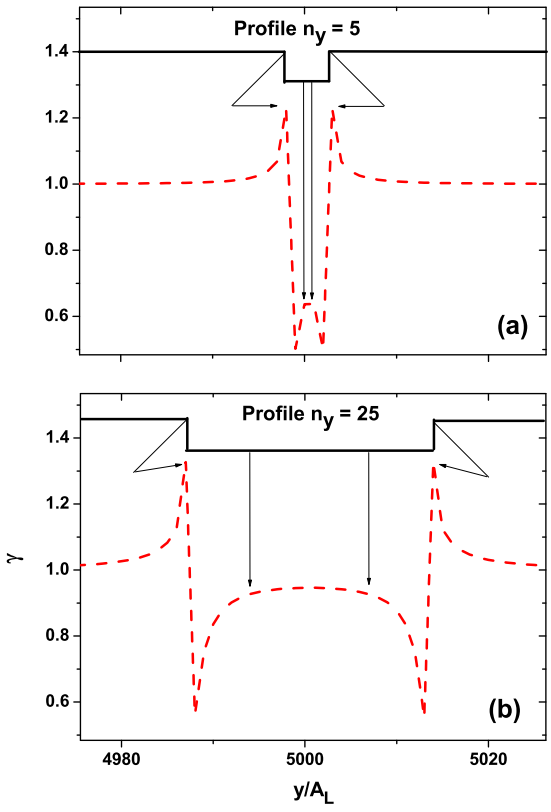


FIG. 5. (Color online) Local enhancement factor, $\gamma$, (dashed line) superimposed to the corresponding fracture profile (solid line), when an homogeneous electric field $F_0 \approx 10^7$ V/cm is applied far away from the profile for two values of the fracture width: (a) $n_y=5$ and (b) $n_y=25$.

In Fig. 6 we present the corresponding values for the ECD, computed with the aid of Eqs. (21) and (22) as a function of the fractrure width, $n_y$, for a value of the external electric field of $F=10^7$ V/cm. These results are very interesting since they reveal the sensibility of the ECD with respect to the small variations of the fracture width. Indeed, the results of Fig. 2 indicated that $J(n_y=15)/J(n_y=5) \approx 55.8$, a very significant deviation from corresponding value of a smooth surface, where $J_{smooth} < 10^{-10}$ A/cm$^2$. The results shown in Fig. 6 provide the geometric set up leading to an optimization of the emitting site. In the current study, we have obtained that the largest value $J(n_y=255) \approx 198.7$ nA/cm$^2$. This result suggests that the presence of irregularities at nanometric scale constitutes an important characteristic of an emitting device, especially when it is designed with the purpose of obtaining a high value of the ECD from a material subjected to low external electric fields. Moreover, this conclusion is in good agreement with the experimental measurements carried out in surface of rough metallic materials. In these experiments, surfaces with a porous structure have been shown to be excellent candidates for low field emitters. For example, in the studies performed by Xiao-Nan *et al.*,[22] these authors obtained interesting results when analyzing the experimental yield of an array of Si structures covered with gold nanoparticles. They found an emission electric field threshold of just a few volt per mi-

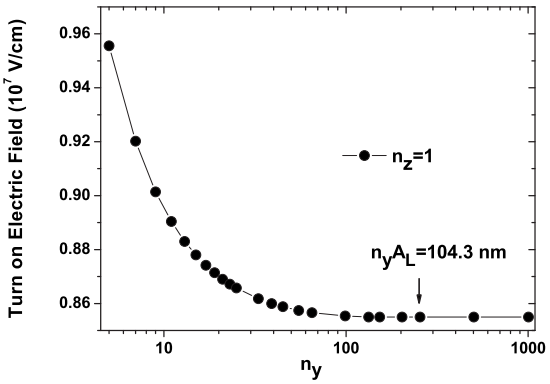


FIG. 7. Turn on external electric field intensity for metallic emitters with fractured surfaces, as a function of $n_y$ in logarithmic scale.

crometer. This shows that, in addition to the parameters associated to the physical and chemical properties of the emitter, the morphology and structure of the surface can play a significant role on the emitting properties of the material, and then they should not be forgotten when designing the corresponding emitting devices.

To conclude this section, we have explored the conditions that determine the threshold value of the electric field for electronic emission, in the case of an emitter with a profile with fracture. Experimentally, a typical threshold value for the ECD current is accepted to be of the order of $J_l = 10^{-10}$ A/cm$^2$; see for example Ref. 23. Figure 7 shows, the dependence of the turn on external electric field with the length of the fracture. The results have been computed using $10^6 \leq F_0 \leq 10^7$ V/cm. Again the arrow indicate the value corresponding to the Ag fracture width. In it, the reduction of the external electric field intensity for which $J=J_l$, especially in the case of an irregular profile formed by fractures, it is clearly appreciated; recall that we are using a logarithmic scale in the horizontal plot. If the values of this field are denoted as $F_l^p$ and $F_l^f$ for the cases of a plane and a surface with a fracture width of $n_y=255$, respectively, our results indicate that $F_l^p/F_l^f \approx 1.16$. This result reflects the importance of considering the roughness at small nanometric scales of metallic surfaces, due to its influence in the corresponding WF, in order to obtain efficient emitter devices arrays operating with high electric currents and low external electric fields.

## IV. SUMMARY AND CONCLUSIONS

In this work we have studied how the geometry of an emitter profile, formed by a succession of rectangular fractures, affects the local values of the WF and the corresponding emitting electronic densities. The classical method of potential images was used for the evaluation of the WF. Our results show that the presence of fracture defects significantly contribute to the ECD calculated along the irregular profile when the electric field distribution at the corresponding surface and variations in the work function are taken into account. The ratio between the emitting threshold values of the external applied field for a plane and a fractured surface with higher horizontal dimensions is $F_l^p/F_l^f \approx 1.16$.

The results of this work allow us to conclude that an increment in the local roughness can lead to a reduction in the value of the corresponding WF of a metal surface in the presence of an electric field. Such influence of the surface morphology seems to provide a satisfactory explanation for the known experimental observation, according to which there is an enhanced corrosion on metals associated with the the surface roughness. It is reasonable to associate this result to the fluctuations in the local WF, leading to the formation of microelectrodes that contribute to speed up the corrosion process.

Finally, we believe that this study also explains the experimental results of Mulyukov *et al.*,[24] who found an increment in the WF of a tungsten emitter after annealing, with a consequent increase in the intensity of $F_l$.

## ACKNOWLEDGMENTS

This work has been supported by MICINN, Spain (Contract Nos. MTM2009-14621 and iMath-CONSOLIDER 2006-32), Conselho Nacional de Desenvolvimento Científico e Tecnológico–CNPq, Brazil (Contract No. 306052/2007-5), and Fundação de Amparo à Pesquisa do Estado da Bahia. TAdA gratefully acknowledges a doctoral grant from AECI (Spain).

[1] J. Li, W. Lei, X. Zhang, X. Shou, Q. Wang, Y. Zhang, and B. Wang, Appl. Surf. Sci. **220**, 96 (2003).
[2] G. N. Fursey, Appl. Surf. Sci. **215**, 113 (2003).
[3] N. A. Burnham, R. J. Colton, and H. M. Pollock, Phys. Rev. Lett. **69**, 144 (1992).
[4] R. Smoluchowski, Phys. Rev. **60**, 661 (1941).
[5] J. Topping, Proc. R. Soc. London, Ser. A **114**, 67 (1927).
[6] J. B. Taylor and I. Langmuir, Phys. Rev. **44**, 423 (1933).
[7] Z. D. Schultz, S. J. Stranick, and I. W. Levin, Appl. Spectrosc. **62**, 1173 (2008).
[8] T. A. de Assis, F. Borondo, R. M. Benito, and R. F. S. Andrade, Phys. Rev. B **78**, 235427 (2008).
[9] R. H. Fowler and L. H. Nordheim, Proc. R. Soc. London, Ser. A **119**, 173 (1928).
[10] E. L. Murphy and R. H. Good, Phys. Rev. **102**, 1464 (1956).
[11] R. G. Forbes, Appl. Phys. Lett. **89**, 113122 (2006).
[12] R. G. Forbes and J. H. B. Deane, Proc. R. Soc. London, Ser. A **463**, 2907 (2007).
[13] J. W. G. Frenken and P. Stoltze, Phys. Rev. Lett. **82**, 3500 (1999).
[14] I. Brodie, Phys. Rev. B **51**, 13660 (1995).
[15] S. Halas and T. Durakiewicz, J. Phys.: Condens. Matter **10**, 10815 (1998).
[16] T. A. de Assis, F. Borondo, C. M. C. de Castilho, F. Brito Mota, and R. M. Benito, J. Phys. D: Appl. Phys. **42**, 195303 (2009).
[17] R. Forbes, Appl. Phys. Lett. **92**, 193105 (2008).
[18] R. Forbes, private communication (24 September 2009).
[19] J. Lapujoulade, *Helium Atom Scattering from Surfaces*, edited by E. Hulpke (Springer-Verlag, Berlin, 1992).
[20] M. J. Mehl and D. A. Papaconstantopoulos, Phys. Rev. B **54**, 4519 (1996).
[21] *CRC Handbook of Chemistry and Physics*, 90th ed. (CRC, Boca Raton, 2010).
[22] F. Xiao-Nan and L. Xin-Jian, Chin. Phys. Lett. **24**, 2335 (2007).
[23] G. Pirio, P. Legagneux, D. Pribat, K. B. K. Teo, M. Chhowalla, G. A. J. Amaratunga, and W. I. Milne, Nanotechnology **13**, 1 (2002).
[24] R. R. Mulyukov and Y. M. Yumaguzin, Dokl. Phys. **49**, 730 (2004).